Second-Order Wave Diffraction by an Axisymmetric Body

Bin Teng* and Shunji Kato**

Abstract

The main difficulty in calculation of third order force is its forcing on the free surface which includes second order potential and its spacial derivatives. Second order potential also obeys an inhomogeneous free-surface boundary condition, and its calculation needs to do an integration on the whole free surface. For third order calculation, its forcing term is needed on a big area on the free surface, and individual calculation of the second order potential at each point in the area is evidently not economic.

This report provides a detailed analysis for the second order diffraction of monochromatic waves by an axisymmetric body in finite water. For wave diffraction from a body of revolution with vertical axis, the report derives a new integral equation, which can cancel the leading singularity in the derivative of ring Green's functions automatically. For the second order potential, the report proposes a forward prediction method to calculate the integration on the free surface. By this method we only need to compute the infinite integration on the free surface directly for a few of points; then an one-step quadrature is applied successively outward from the body for potentials at other points. To get accurate results, different approaches are also used to deal with singularities in the ring Green's functions in the integration both on the body surface and free surface. The method has been implemented for body of revolution with vertical axes, but the theory is also available for arbitrary bodies.

Numerical examination is also made to validate the numerical code by comparing second order force and moment on uniform and truncated cylinders and second order diffraction potential on the free surface with some published results. The comparison shows that the present results have a good agreement with those results. At last, the method is used to compute the second order wave elevation around uniform and truncated cylinders.

* Associated professor, Dalian University of Technology, China
Stay at Ocean Engineering Division as a STA(Science and Technology Agency) fellow from March,1995 till August, 1996.
** Ocean Engineering Division
Received on August 26, 1996
Accepted on March 12, 1997

Contents

1. Introduction

It was observed in model tests and prototype experiments that tension leg platforms (TLPs) and gravity based structures (GBS) experience sudden bursts of highly amplified resonant activities during storms. This phenomenon is called as the 'ringing'. The ringing phenomenon will induce extreme stress in tethers of TLP, and even induces tethers breaking. It was found that ringing occurs at low frequency non-breaking waves and ringing periods are about 3-5 times of the period of the corresponding incident waves. This means that third order force is an exciting source for ringing and its calculation will be significant in predicting ringing phenomenon.

Nonlinear problems are characterized by forcing term in their boundary conditions. For the second order potential, the forcing term on the free surface only includes first order potentials, which can be represented by some simple ways. However, the third order forcing term on the free surface includes both first and second order potentials. The difficulty in calculating third order forcing term is the complexity and time-consuming in the calculation of second order potential, which is needed on the whole free surface or a big area. Usually, an integral equation method is used to compute the second order velocity potential, in which integrations have to be carried out on both body and free surfaces.

To get rid of the potential at the considering order from the integration on the free surface and the sea bed, an oscillating source with corresponding frequency is usually applied as the Green's function. The basic representation of the Green's function is written in a function of the Bessel function of the first kind of zero order. Kriebel (1990) used this representation in calculation of second wave elevation around a uniform cylinder. After using Graf's addition theorem to represent the Bessel function by the radii of source and field points in a polar coordinate system located at origin of the cylinder, we can get an unanimous representation with multiplications of functions of the radii of field and source points, no matter the radius of field point is larger than the one of source point or not. Thus, we can integrate the forcing term on the free surface with the functions only relative to the radius of field point to get a wave number spectrum. Then, second order potential can be represented by the wave number spectrum in an explicit form. To calculate the third order forcing term on the free surface, Teng and Kato (1996) tried to use this method to compute second order diffraction potential from an axisymmetric body. They found that the wave number spectrum goes to infinite at a wave number of twice of incident wave number when water depth is not infinity. The reason is that there is a component with twice of incident wave number in the second order forcing term on the free surface, which is called as the 'locked wave' by Molin(1979). Multiplication of the second order forcing term with Bessel functions at that wave number will give constant contribution with the increase of distance. Applied some techniques to deal with the infinity, Teng and Kato (1996) found that it is still hard to get a good agreement with Eatock Taylor and Hung's (1987) on the second order forces on uniform cylinders. The reason is that the wave number spectrum from this method converges slowly at high wave number, especially its derivatives.

To compute second order potential and forces, Hunt and Baddour (1981) and Hunt and Williams (1982) applied Weber transformation method, which is similar as the method by applying the above mentioned Green's function. Later, it was found that their results are not reliable. It has been doubted that their velocity potential is incomplete. Recently, Newman (1996) studied the problem again by the same method. For second

order potential on body surface of a uniform cylinder, he used Wronskians and transformation of integration contour to overcome the numerical inefficiency. Then, he managed to get a good agreement with Eatock Taylor and Hung's on second order forces.

Another representation of Green's function is of the modified Bessel functions, which is gotten by transformation of integrating contour. The Green's function in this form converges quickly, but the problem is that it has different definitions when radius of source point is larger than the one of field point or vice versa. For computing the second order force on bodies, this representation does not give too much troubles. However, for second order potential on the free surface, the integration domain on the free surface has to be separated into two different ranges according to the radius of source point. Thus, the second order diffraction potentials at different positions can not be represented by an explicit representation. Chau and Eatock Taylor (1992) used a similar Green's function, which also satisfies the body surface condition, and developed a semi-analytic solution for uniform cylinder. They used this method to compute second order wave elevation in the near field surrounding the cylinder. Huang and Eatock Taylor (1996) even developed a semi-analytic solution for truncated cylinders. For third order calculation, second order potential is needed on the whole free surface or in a very big domain. Calculation by this method directly seems very expansive, as an infinite integration has to be carried out for each point. Malenica and Molin (1995) made some improvement on this method in their third order calculation. They applied a forward moving approach to predict the integration associated with Hankel function from smaller radius to bigger one step by step. But for the parts associated with an infinite summation of the modified Bessel functions, they still used the direct integration method as Chau and Eatock Taylor did.

The present work proposes an one-step forward prediction method for calculating the terms associated with modified Bessel functions. Special concerns are also paid on the treatment for the logarithmic singularity in the ring Green's functions. By this approach, the second order potential can be calculated much more efficiently in a big area, like to form the forcing term for third order problem. The method has been implemented for axisymmetric bodies, and no difficulty has been found for extending it to arbitrary bodies, like TLPs.

2. Free Surface Condition

We define a right-handed coordinate system *(x, y, z)*, with origin at the center of the body, *z=0* on the still free surface and the z-axis pointing upward (see Figure 1). The fluid is assumed to be homogenous and incompressible, and irrotational. There exists a velocity potential that satisfies the Laplace equation and the nonlinear free-surface boundary condition on

$$\Phi_{tt} + g\Phi_z + \frac{\partial}{\partial t}[\nabla\Phi\cdot\nabla\Phi] + \frac{1}{2}\nabla\Phi\cdot\nabla(\nabla\Phi\cdot\nabla\Phi) = 0 \tag{1}$$

the free surface $z=\zeta(x,y,t)$, defined by

$$\zeta = \frac{1}{g}\Phi_t - \frac{1}{2g}[\nabla\Phi\cdot\nabla\Phi] \tag{2}$$

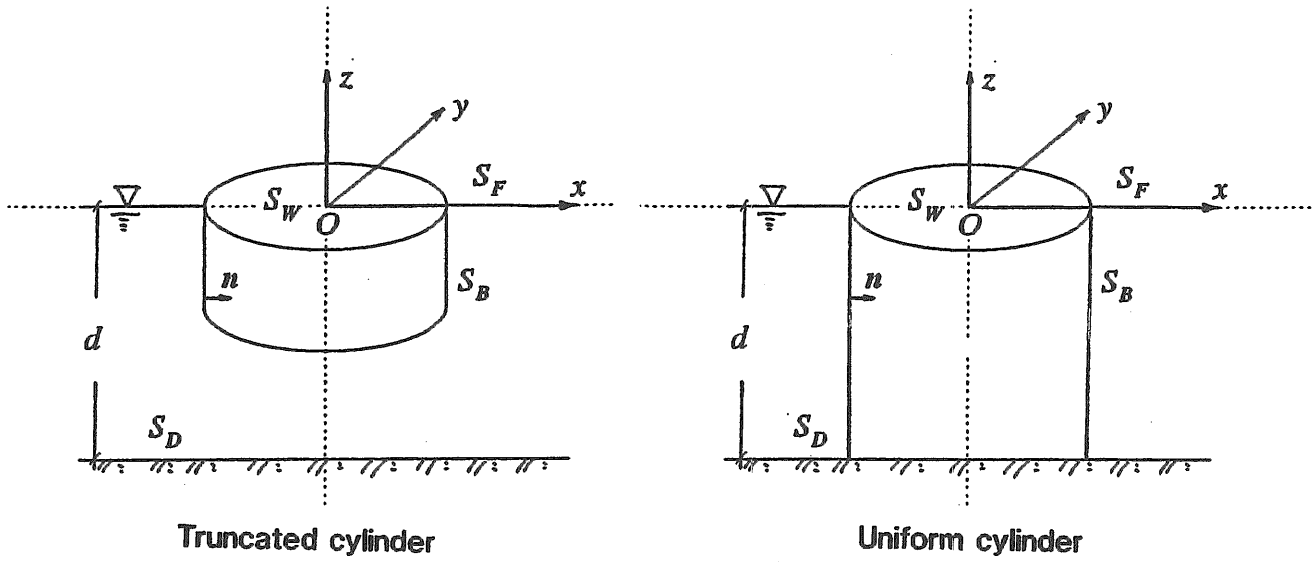

Figure 1. Definition sketch

Under the assumption of weak non-linearity, we can write the wave velocity potential as a perturbation series with respect to wave slope parameter $\varepsilon = kA$

$$\Phi = \varepsilon \Phi^{(1)} + \varepsilon^2 \Phi^{(2)} + \varepsilon^3 \Phi^{(3)} + \ldots \tag{3}$$

We assume that the incident monochromatic waves have an incident frequency ω. To solve the ringing phenomena, the first, second and third order harmonic potentials with the frequencies of $\omega_1 = \omega$, $\omega_2 = 2\omega$ and $\omega_3 = 3\omega$ are only considered. We separate the time dependencies explicitly, and write potentials at each order of ε as

$$\Phi^{(j)}(x,y,z,t) = Re[\phi^{(j)}(x,y,z)e^{-i\omega_j t}] \tag{4}$$

After expanding eq. (1) into a perturbation series and collecting terms at the same order of ε, we can write the free surface conditions for the velocity potentials at each order of ε as

$$\nu_j \phi^{(j)} + \phi_z^{(j)} = q^{(j)} \qquad on\ z=0 \tag{5}$$

where

$$\nu_j = \omega_j^2 / g \tag{6}$$

and the forcing terms at each order of ε

$$
\begin{aligned}
q^{(1)} &= 0 \\
q^{(2)} &= -\frac{i\omega}{2g}\phi^{(1)}\left(-\frac{\omega^2}{g}\phi_z^{(1)}+\phi_{zz}^{(1)}\right)+\frac{i\omega}{g}\nabla\phi^{(1)}\cdot\nabla\phi^{(1)} \\
q^{(3)} &= \frac{3i\omega}{g}\nabla\phi^{(1)}\cdot\nabla\phi^{(2)}-\frac{i\omega}{2g}\phi^{(1)}\left(\phi_{zz}^{(2)}-4\nu\phi_z^{(2)}\right)-\frac{i\omega}{g}\phi^{(2)}\left(\phi_{zz}^{(1)}-\nu\phi_z^{(1)}\right) \\
&\quad -\frac{1}{8g}\nabla\phi^{(1)}\cdot\nabla\left(\nabla\phi^{(1)}\cdot\nabla\phi^{(1)}\right)-\frac{\nu}{g}\phi^{(1)}\nabla\phi^{(1)}\cdot\nabla\phi_z^{(1)} \\
&\quad +\frac{1}{g}\left(\frac{\nu}{4}\phi^{(1)}\phi_z^{(1)}+\frac{1}{8}\nabla\phi^{(1)}\cdot\nabla\phi^{(1)}\right)\left(\phi_{zz}^{(1)}-\nu\phi_z^{(1)}\right)
\end{aligned}
\tag{7}
$$

It can be seen that the third order forcing term includes both first and second order potential.

3. Integral Equation

For convenience in numerical calculation, we separate velocity potential into incident and diffraction potentials

$$
\phi^{(j)} = \phi_I^{(j)} + \phi_D^{(j)} \tag{8}
$$

By applying an oscillating source with frequency ω_j as the Green's function, we can obtain an integral equation for jth order diffraction potential as

$$
\begin{aligned}
&\alpha\,\phi_D^{(j)}(x_0) - \iint_{S_B}\frac{\partial G(x;x_0;\omega_j)}{\partial n}\phi_D^{(j)}(x)\,ds \\
&\qquad = \iint_{S_B} G(x;x_0;\omega_j)\frac{\partial\phi_I^{(j)}}{\partial n}ds - \iint_{S_F} G(x;x_0;\omega_j)\,q_D^{(j)}\,ds
\end{aligned}
\tag{9}
$$

where S_B and S_F denote the body and free surface, and $q_D{}^{(j)}$ is the difference between the total forcing term and the forcing one for incident waves

$$
q_D^{(j)} = q^{(j)} - q_I^{(j)} \tag{10}
$$

The positive direction of the normal to the body surface is defined as being out of the fluid. To weaken the singularity in the integration of derivative of the Green's function, we add another equation obtained inside the body (Eatock Taylor and Chau, 1992, and Teng and Eatock Taylor, 1995) and get a new equation as

$$(1-\nu_j\iint_{S_W} Gds)\phi_D^{(j)}(x_0)+\iint_{S_B}\frac{\partial G}{\partial n}(\phi_D^{(j)}(x_0)-\phi_D^{(j)}(x))\,ds$$
$$=\iint_{S_B} G\frac{\partial\phi_I^{(j)}(x)}{\partial n}ds-\iint_{S_F} Gq_D^{(j)}\,ds \tag{11}$$

where S_W is the inner free surface. For axisymmetric body, we expand the velocity potential and the Green's function into series

$$\phi_D^{(j)}(x_0)=\sum_{m=0}^{\infty}\varepsilon_m\phi_{Dm}^{(j)}(r_0)\cos m\theta_0 \qquad \phi_D^{(j)}(x)=\sum_{m=0}^{\infty}\varepsilon_m\phi_{Dm}^{(j)}(r)\cos m\theta \tag{12}$$
$$G(x;x_0)=\sum_{m=0}^{\infty}\varepsilon_m G_m(r,z;r_0,z_0)\cos m(\theta-\theta_0)$$

where ε_m is the coefficient of Neumann's polynomial(=1 when m=0, 2 when m>0), e.g. see Watson,1966. Then, the integral equation for the mth mode in azimuthal angle θ of jth order potential can be obtained as

$$[\frac{1}{2\pi}-\nu_j\int_{\Gamma_W} G_0 r\,dr]\phi_{Dm}^{(j)}(r_0)-\int_{\Gamma_B}[\frac{\partial G_0}{\partial n}\phi_{Dm}^{(j)}(r_0)-\frac{\partial G_m}{\partial n}\phi_{Dm}^{(j)}(r)]r\,dl$$
$$=\int_{\Gamma_B} G_m\frac{\partial\phi_{Im}^{(j)}}{\partial n}r\,dl+\int_a^{\infty} G_m q_{Dm}^{(j)}(r)\,r\,dr \tag{13}$$

where Γ_B and Γ_W are the traces of S_B and S_W (see Figure 2), and the ring Green's function G_m is

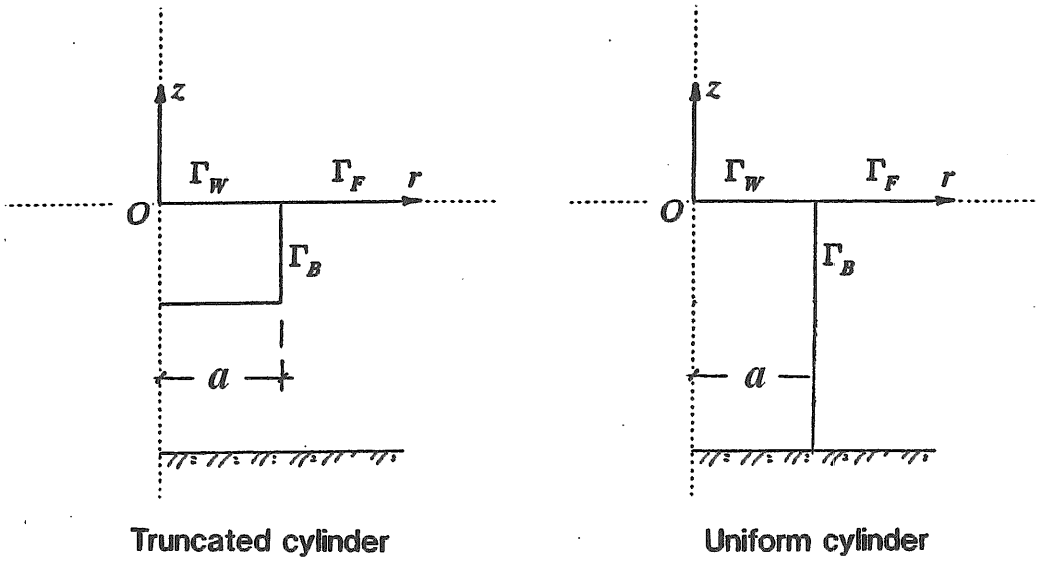

Figure 2. Integrating contour for axisymmetric body

$$G_m = -\frac{i}{2} C_0 H_m(k_j r_>) J_m(k_j r_<) Z_0(k_j z) Z_0(k_j z_0)$$
$$-\frac{1}{\pi} \sum_{n=1}^{\infty} C_n K_m(\kappa_{jn} r_>) I_m(\kappa_{jn} r_<) Z_n(\kappa_{jn} z) Z_n(\kappa_{jn} z_0) \qquad \text{where } r_> > r_< \tag{14}$$

k_j and κ_{jn} are defined by dispersion equations of

$$\nu_j = k_j \tanh(k_j d) \qquad \nu_j = -\kappa_{jn} tg(\kappa_{jn} d) \tag{15}$$

where d is the water depth. The eigenfunctions in z-direction are defined by

$$Z_0(k_j z) = \frac{\cosh k_j(z+d)}{\cosh k_j d}, \qquad Z_n(\kappa_{jn} z) = \frac{\cos \kappa_{jn}(z+d)}{\cos \kappa_{jn} d} \tag{16}$$

and the factor C_0 and C_n are

$$C_0 = [2 \int_{-d}^{0} Z_0^2(k_j z) dz]^{-1}, \qquad C_n = [2 \int_{-d}^{0} Z_n^2(\kappa_{jn} z) dz]^{-1} \tag{17}$$

The ring-source potential and its derivative have been investigated by a number of researchers (Fenton, 1978; Hulme, 1983; Kim and Yue, 1989). It was found that the ring sources at each mode have the same logarithmic singularity when field point is close to the source point; and the leading singularities in their derivatives have the same form as the reverse of the distance between field point and source point. Thus, the leading term of singularity in equation (13) can be canceled each other. Other weak singularities are dealt with by suitable coordinate transformation (Telles, 1987).

For the second order potential, if the minimum radius of free surface is larger than or equal to the maximum radius of the body (otherwise, we should divide the free surface into different ranges), the integral on the free surface can be written as

$$I_F(r_0, \theta_0, z_0) = -\int_a^{\infty} r dr \sum_{m=0}^{\infty} \varepsilon_m q_{Dm}^{(2)}(r) \cos m\theta_0$$
$$[\frac{i\pi}{2} C_0 H_m(k_2 r_>) J_m(k_2 r_<) Z_0(k_2 z_0) + \sum_{n=1}^{\infty} C_n K_m(\kappa_n r_>) I_m(\kappa_n r_<) Z_n(\kappa_n z_0)] \tag{18}$$

where $\kappa_n = \kappa_{2n}$ for brevity. By defining

$$S_{1m0}(a) = \frac{i\pi}{2} \int_a^{\infty} q_{Dm}^{(2)}(r) H_m(k_2 r) r dr, \qquad S_{1mn}(a) = \int_a^{\infty} q_{Dm}^{(2)}(r) K_m(\kappa_n r) r dr, \tag{19}$$

we can write the above integral equation as

$$I_F(r_0, \theta_0, z_0) = -\sum_{m=0}^{\infty} \varepsilon_m [C_0 S_{1m0}(a) J_m(k_2 r_0) Z_0(k_2 z_0) + \sum_{n=1}^{\infty} C_n S_{1mn}(a) I_m(\kappa_n r_0) Z_n(\kappa_n z_0)] \cos m\theta_0 \tag{20}$$

Thus, for the second order potential on the body surface, integration on the free surface is only needed to run once.

The infinite integration of S_{1mn} $(n>0)$ converges quickly with the increase of the integration range as the modified Bessel function K_m decays at an exponential rate. However, the infinite integration of S_{1m0} is oscillating and converges slowly with the increase of integrating distance. A method widely used for its calculation is to divide the integration range into two parts. In the inner domain, a direct quadrature is used, and in the outer domain an analytic method is used to integrate it to infinity, after some asymptotic approximations have been used for Hankel functions.

4. Second Order Potential on Free Surface

For the second order potential at a point not close to the body, the following integral equation can be used to compute second order potential directly

$$\phi_D^{(2)}(x_0,0) - \iint_{S_B} \frac{\partial G}{\partial n} \phi_D^{(2)}(x,z)\, ds = \iint_{S_B} G \frac{\partial \phi_I^{(2)}(x,z)}{\partial n} ds - \iint_{S_F} G q_D^{(2)}\, ds \tag{21}$$

For axisymmetric body, the integral equation for mth mode with respect to azimuthal angle θ can be written as

$$\frac{1}{2\pi}\phi_{Dm}^{(2)}(r_0,0) = \int_{\Gamma_B} \frac{\partial G_m}{\partial n} \phi_{Dm}^{(2)}(r,z)\, r dl + \int_{\Gamma_B} G_m \frac{\partial \phi_{Im}(r,z)}{\partial n} r dl - \int_a^{\infty} G_m q_{Dm}^{(2)} r dr \tag{22}$$

However, when the computed point is close to the body surface, there are some quasi- singularities in the body integration. Direct use of the above integral equation will not give accurate results. For weakening the quasi-singularities, we add another integral equation

$$-\nu_2 \iint_{S_W} G(x, x_0) ds \phi_D(x^*) + \iint_{S_B} \frac{\partial G(x, x_0)}{\partial n} \phi_D^{(2)}(x^*) ds = 0 \tag{23}$$

to the above equation, where

$$x^* = a\cos\theta_0 , \qquad for \quad x_0 = r_0 \cos\theta_0 \tag{24}$$

is the closest point to the computed point on the water line. It yields a new integral equation

$$\phi_D^{(2)}(x_0) - \nu_2 \iint_{S_W} G ds\, \phi_D^{(2)}(x^*) + \iint_{S_B} \frac{\partial G}{\partial n} (\phi_D^{(2)}(x^*) - \phi_D^{(2)}(x)) ds$$
$$= \iint_{S_B} G \frac{\partial \phi_I^{(2)}(x)}{\partial n} ds - \iint_{S_F} G\, q_D^{(2)}\, ds \tag{25}$$

We expand the potentials into series

$$\phi_D^{(2)}(x_0) = \sum_{m=0}^{\infty} \varepsilon_m \phi_{Dm}^{(2)}(r_0) cosm\theta_0, \qquad \phi_D^{(2)}(x^*) = \sum_{m=0}^{\infty} \varepsilon_m \phi_{Dm}^{(2)}(a) cosm\theta_0, \tag{26}$$

Then, another integral equation can be obtained for the mth mode of second order potential as

$$\frac{1}{2\pi}\phi_{Dm}^{(2)}(r_0) = \nu_2 \int_{\Gamma_W} G_0 r dr\, \phi_{Dm}^{(2)}(a) - \int_{\Gamma_B} [\frac{\partial G_0}{\partial n}\phi_{Dm}^{(2)}(a) - \frac{\partial G_m}{\partial n}\phi_{Dm}^{(2)}(r)] r dl$$
$$+ \int_{\Gamma_B} G_m \frac{\partial \phi_{Im}^{(2)}}{\partial n} r dl - \int_a^{\infty} G_m\, q_{Dm}^{(2)}\, r\, dr \tag{27}$$

This equation will weaken the leading term of quasi-singularity, and the other quasi- singularities will still be dealt with by coordinate transformation.

5. Numerical Implementation

For second order potential on the body surface and in the fluid domain, two integrations have to be carried out both on body surface and free surface when an integral equation method is used. Direct calculation of those integrations is very expansive when second order potential is needed in a big area, like to form the third order forcing term on the free surface. Thus, some techniques have to be applied to aim at a speedup of the calculation. Besides the inefficiency in calculation of the integration on the free surface, the singularity in the ring Green's function has to be dealt with carefully. The ring Green's function is represented by an infinite summation of modified Bessel functions, and simple truncation will induce great inaccuracy when field point approaches to the source point. To calculated those integration accurately, some special approaches are used.

5.1 The integration on the free surface

Substituting the ring Green's function into the above integration, the integration on the free surface can be written as

$$I_{Fm}(r_0, \theta_0, 0) = -\int_a^{\infty} r dr\, q_{Dm}^{(2)}(r) [i\pi C_0 H_m(k_2 r_>) J_m(k_2 r_<)$$
$$+ 2\sum_{n=1}^{\infty} C_n K_m(\kappa_n r_>) I_m(\kappa_n r_<)] \tag{28}$$

The Green's function is represented by multiplies of Bessel function and an infinite summation of modified Bessel functions. In numerical calculation the infinite summation has to be truncated at a big value N. As pointed out by Fenton (1978), there is a logarithmic singularity in the ring Green's function, and simple truncation will induce some inaccuracy. We define each term of the multiplication of modified Bessel function as

$$L_{mn} = 2C_n K_m(\kappa_n r_>) I_m(\kappa_n r_<) Z_n(\kappa_n z) \tag{29}$$

The limitation of L_{mn} term at large n is

$$L_{mn} \to L_{mn}^s = \frac{1}{n\pi}\frac{1}{\sqrt{rr_0}} \exp(-\frac{n\pi}{d}|r-r_0|)\cos\frac{n\pi z}{d} \tag{30}$$

and the infinite sum of L_{mn}^s can be written as

$$\begin{aligned} L_m^s &= \sum_{n=1}^{\infty} L_{mn}^s = \sum_{n=1}^{\infty} \frac{1}{n\pi}\frac{1}{\sqrt{rr_0}} \exp(-\frac{n\pi}{d}|r-r_0|) \\ &= \frac{-1}{2\pi\sqrt{rr_0}} \ln[1-2\exp(-\frac{\pi}{d}|r-r_0|)\cos\frac{\pi z}{d} + \exp(-\frac{2\pi}{d}|r-r_0|)] \end{aligned} \tag{31}$$

When field point is close to the source point, we expend the exponential and cosine functions into Taylor series and can find that it is a logarithmic singularity of

$$L_m^s \sim \frac{-1}{2\pi\sqrt{rr_0}} \ln[\frac{\pi^2}{d^2}(z^2+(r-r_0)^2)] \tag{32}$$

To remove the logarithmic singularity, we write the infinite integration of modified Bessel function as

$$\begin{aligned} \sum_{n=1}^{\infty}\int_a^{\infty} L_{mn}(r) q_{Dm}^{(2)}(r) r\,dr &= \sum_{n=1}^{\infty}\int_a^{\infty} L_{mn}(r) q_{Dm}^{(2)}(r) r\,dr - \sum_{n=1}^{\infty}\int_{r_0-\Delta r_1}^{r_0+\Delta r_2} L_{mn}^s(r) q_{Dm}^{(2)}(r) r\,dr \\ &+ \int_{r_0-\Delta r_1}^{r_0+\Delta r_2} L_m^s(r) q_{Dm}^{(2)}(r) r\,dr \end{aligned} \tag{33}$$

Outside the range $(r-\Delta r_1, r+\Delta r_2)$, the higher modes in the first integration decay quickly and the summation can be truncated at a big value N; inside the range $(r-\Delta r_1, r+\Delta r_2)$ the integrand in the first two terms will be close to and cancel each other for big modes. Truncation at the big N will also give a good approximation. Thus, we can write the integration as

$$\sum_{n=1}^{\infty}\int_{a}^{\infty} L_{mn}(r)q_{Dm}^{(2)}(r)rdr \simeq \sum_{n=1}^{N}\int_{a}^{\infty} L_{mn}(r)q_{Dm}^{(2)}(r)rdr - \sum_{n=1}^{N}\int_{r_0-\Delta r_1}^{r_0+\Delta r_2} L_{mn}^{s}(r)q_{Dm}^{(2)}(r)rdr + \int_{r_0-\Delta r_1}^{r_0+\Delta r_2} L_{m}^{s}(r)q_{Dm}^{(2)}(r)rdr \tag{34}$$

For the third term, a coordinate transform

$$r=\frac{1}{2}\Delta r\xi+\frac{1}{2}(2r_0+\Delta r), \qquad \xi=\frac{1}{2}\eta^2+\eta-\frac{1}{2}, \qquad dr=\frac{1}{2}\Delta r(\eta+1) \tag{35}$$

is used to remove the singularity. Then, we represent the integration on the free surface as

$$I_{Fm}(r_0,0) = -C_0(S_{1m0}(r_0)J_m(k_2r_0)+S_{2m0}(r_0)H_m(k_2r_0)) - \sum_{n=1}^{N} C_n(S_{1mn}(r_0)e^{-\kappa_n r_0}I_m(\kappa_n r_0)+S_{2mn}(r_0)e^{\kappa_n r_0}K_m(\kappa_n r_0)) + \sum_{n=1}^{N} V_{mn}(r_0) - V_{m0}(r_0) \tag{36}$$

The functions in the above equation are defined by

$$S_{1m0}(r_0)=\frac{i\pi}{2}\int_{r_0}^{\infty} q_{Dm}^{(2)}(r)H_m(k_2r)rdr, \qquad S_{1mn}(r_0)=\int_{r_0}^{\infty} q_{Dm}^{(2)}(r)K_m(\kappa_n r)rdre^{\kappa_n r_0},$$
$$S_{2m0}(r_0)=\frac{i\pi}{2}\int_{a}^{r_0} q_{Dm}^{(2)}(r)J_m(k_2r)rdr, \qquad S_{2mn}(r_0)=\int_{a}^{r_0} q_{Dm}^{(2)}(r)I_m(\kappa_n r)rdre^{-\kappa_n r_0}. \tag{37}$$

and

$$V_{m0}(r_0)=-\frac{1}{2\pi}\int_{r_0-\Delta r_1}^{r_0+\Delta r_2} q_{Dm}^{(2)}(r)\ln[1-\exp(-\frac{\pi}{d}|r-r_0|)]\sqrt{\frac{r}{r_0}}dr$$
$$V_{mn}(r_0)=\frac{1}{2n\pi}\int_{r_0-\Delta r_1}^{r_0+\Delta r_2} q_{Dm}^{(2)}(r)\exp(-\frac{\pi}{nd}|r-r_0|)\sqrt{\frac{r}{r_0}}dr \tag{38}$$

Here, the exponential functions are applied to multiply with modified Bessel functions to guarantee the integrand not to overflow from both upper and lower limits of computers at large variable.

The integration in the function V_{mn} is localized in a small range $(r-\Delta r_1, r+\Delta r_2)$, and can be calculated easily. However, the integrations in S_{1mn} and S_{2mn} have to be carried out from the body to infinity. Direct calculation will be very expansive, especially when calculation for many points is needed. Here, a one-step forward prediction method is applied. By this method, after we have gotten those functions at a point r_0, the functions at next point r_1, which is close to r_0, can be obtained by

$$S_{1m0}(r_1) = \frac{i\pi}{2}\int_{r_1}^{\infty} q_{Dm}^{(2)}(r) H_m(k_2 r) r dr = S_{1m0}(r_0) - \frac{i\pi}{2}\int_{r_0}^{r_1} q_{Dm}^{(2)}(r) H_m(k_2 r) r dr$$
$$S_{2m0}(r_1) = \frac{i\pi}{2}\int_{a}^{r_1} q_{Dm}^{(2)}(r) J_m(k_2 r) r dr = S_{2m0}(r_0) + \frac{i\pi}{2}\int_{r_0}^{r_1} q_{Dm}^{(2)}(r) J_m(k_2 r) r dr \quad (39)$$

and

$$S_{1mn}(r_1) = \int_{r_1}^{\infty} q_{Dm}^{(2)}(r) K_m(\kappa_n r) r dr = S_{1mn}(r_0) e^{\kappa_n(r_1 - r_0)} - \int_{r_0}^{r_1} q_{Dm}^{(2)}(r) K_m(\kappa_n r) r dr e^{\kappa_n r_1}$$
$$S_{2mn}(r_1) = \int_{a}^{r_1} q_{Dm}^{(2)}(r) J_m(\kappa_n r) r dr = S_{2mn}(r_0) e^{-\kappa_n(r_1 - r_n)} + \int_{r_0}^{r_1} q_{Dm}^{(2)}(r) I_m(\kappa_n r) r dr e^{-\kappa_n r_1} \quad (40)$$

This method can save a lot of computing effort. But after a number of steps, the prediction will lose accuracy, and even diverse. A remedy to solve this problem is just to use the direct integration method to compute them again before a tolerant error has been accumulated. The number of steps used in forward prediction will be determined by a series forehead numerical examination, and is different for different modes.

For the integrations of Hankel and Bessel functions, the terms called as S_{1m0} and S_{2m0} in this paper, Malenica (1994) used a similar method to deal with them. But for the infinite summation of modified Bessel functions, S_{1mn} and S_{2mn} in this paper, Malenica still used the direct integration method to compute them. Another distinct difference between the present method and Malenica's is the approach used to treat the singularity in the ring Green's function. The present method only adds an auxiliary integration in a small adjacent area of the source point, but Malenica's is to add an auxiliary integration in the same area as the original integration.

5.2 The integration on the body surface

For those points not close to body surface, we apply equation (21) to compute the second order potential. The integration on the body surface can be written as

$$I_{Bm}(r_0,0) = \int_{\Gamma_B} [\phi_{Dm}^{(2)}(r,z) \frac{\partial G_m(r,z;r_0,0)}{\partial n} + \frac{\partial \phi_{Im}^{(2)}(r,z)}{\partial n} G_m(r,z;r_0,0)] r dl \quad (41)$$

After integrating with respect to the coordinates of field point on the body surface, the body surface integration can be simply written as

$$I_{Bm}(r_0,0) = U_{m0} H_m(k_2 r_0) + \sum_{n=1}^{\infty} U_{mn} K_m(\kappa_n r_0) \quad (42)$$

where

$$U_{m0} = -\frac{iC_0}{2}\int_{\Gamma_B}[\phi^{(2)}_{Dm}(r,z)\,(\frac{\partial J_m(k_2 r)}{\partial r}n_r Z_0(k_2 z)+J_m(k_2 r)\frac{\partial Z_0(k_2 z)}{\partial z}n_z)$$
$$+\frac{\partial \phi^{(2)}_{Im}(r,z)}{\partial n}J_m(k_2 r)Z_0(k_2 z)]\,r\,dl \qquad (43)$$
$$U_{mn} = -\frac{C_n}{\pi}\int_{\Gamma_B}[\phi^{(2)}_{Dm}(r,z)\,(\frac{\partial I_m(\kappa_n r)}{\partial r}n_r Z_n(\kappa_n z)+I_m(\kappa_n r)\frac{\partial Z_n(\kappa_n z)}{\partial z}n_z)$$
$$+\frac{\partial \phi^{(2)}_{Im}(r,z)}{\partial n}I_m(\kappa_n r)Z_n(\kappa_n z)]\,r\,dl$$

For those points close to body surface, a direct integration method is performed with an application of equation (27).

6. Numerical Results

6.1 Second order force

To ensure the numerical code reliable, we first make a comparison on the second order force with some published results.

After we have resolved the second order potential, the second order wave force and moment can be obtained by direct integration of hydrodynamic pressure on the body surface with an approximation to second order in ε. After some mathematical derivation, the equation of the second order generalized force on a vertically piercing fixed body in monochromatic waves can be written as

$$F_T^{(2)} = Re[(f_p^{(2)}+f_q^{(2)})e^{-2i\omega t}] \qquad (44)$$

where

$$f_p^{(2)} = \frac{\rho}{2}\int\int_{S_B} i\omega\,(\phi_I^{(2)}+\phi_D^{(2)})\,n\,ds \qquad (45)$$

is the contribution from the second order velocity potentials; and is the contribution from quadratic multiplication of first order velocity potentials and height of water surface ζ, where $n=(n_r, n_z, (z-z_c)n_r-rn_z)$, z_c is the center of mass and C_W is the water line.

For axisymmetric body, we rearrange the quadratic multiplication of first order terms as

$$\nabla\phi^{(1)}\cdot\nabla\phi^{(1)} = \sum_{m=0}^{\infty}\varepsilon_m\varphi_m\cos m\theta \qquad \zeta^{(1)}\zeta^{(1)} = \sum_{m=0}^{\infty}\varepsilon_m\eta_m\cos m\theta \qquad (47)$$

and write the second order surge force as

$$f_{qx}^{(2)} = -\frac{\pi}{2}\int_{\Gamma_B} \rho\, \varphi_1 n_r r dl + \frac{\pi}{2}\rho g a \eta_1 n_r|_{R=a}$$
$$f_{px}^{(2)} = -\frac{\pi}{2}\int_{\Gamma_B} \rho\, \phi_1^{(2)} n_r r dl \tag{48}$$

the second order heave force as

$$f_{qz}^{(2)} = -\frac{\pi}{2}\int_{\Gamma_B} \rho\, \varphi_0 n_z r dl + \frac{\pi}{2}\rho g a \eta_0 n_z|_{R=a}$$
$$f_{pz}^{(2)} = -\frac{\pi}{2}\int_{\Gamma_B} \rho\, \phi_0^{(2)} n_z r dl \tag{49}$$

and the second order pitch moment as

$$m_{qy}^{(2)} = -\frac{\pi}{2}\int_{\Gamma_B} \rho\, \varphi_1 n_r r dl + \frac{\pi}{2}\rho g a \eta_1 n_r|_{R=a}$$
$$m_{py}^{(2)} = -\frac{\pi}{2}\int_{\Gamma_B} \rho\, \phi_1^{(2)} n_r r dl \tag{50}$$

Tables 1-3 are comparison with Eatock Taylor and Hung's (1987) results on the part of second order force from second order potential, $f_p^{(2)}$, on uniform cylinders in different water depth d/a= 1.0, 3.0 and 10.0. The Eatock Taylor and Hung's results have been rearranged by summing up of the data in the last three columns of their paper. The meshes used in the present calculation are 4, 16 and 40 elements respectively for the three cylinders. It can be seen that for all of the three cylinders and in the all frequency range of the calculation, the present results have a good agreement with Eatock Taylor and Hung's.

Table 1. Comparison on f_p, the part of second order forces from second potential, on a uniform cylinder h/a=1.0.

ka	Present Results		Ref. (1)	
	Re	Im	Re	Im
0.25	.7126E+05	-.3640E+06	.7144E+05	-.3649E+06
0.50	.4469E+05	-.9970E+05	.4477E+05	-.9992E+05
0.75	.1138E+05	-.3294E+05	.1140E+05	-.3300E+05
1.00	.8931E+04	-.1181E+05	.8937E+04	-.1183E+05
1.25	.1802E+05	-.3080E+04	.1804E+05	-.3038E+04
1.50	.2679E+05	-.1115E+04	.2687E+05	-.1116E+04

Table 2. Comparison on f_h, the part of second order forces from second potential, on a uniform cylinder h/a=3.0.

ka	Present Results		Ref. (1)	
	Re	Im	Re	Im
0.25	.1268E+05	-.3118E+05	.1272E+05	-.3133E+06
0.50	.6409E+04	.8404E+04	.6431E+04	.8417E+04
0.75	.8837E+04	.1819E+05	.8868E+04	.1824E+05
1.00	.1963E+05	.1961E+05	.1966E+05	.1979E+05
1.25	.3385E+05	.1585E+05	.3396E+05	.1597E+05
1.50	.4521E+05	.7071E+04	.4538E+05	.7098E+04

Table 4 is the second order pitch moment with respect to the free surface on those cylinders. For this case, we have not found available published results to compare with. From the table, it can be seen that the component from the second order potential is the dominant part. In shallow water, large moment occurs at low frequency; in deep water, large moment occurs at high frequency.

Table 3. Comparison on f_h, the part of second order forces from second potential, on a uniform cylinder h/a=10.0.

ka	Present Results		Ref. (1)	
	Re	Im	Re	Im
0.25	.7126E+05	-.3640E+06	.7144E+05	-.3649E+06
0.50	.4469E+05	-.9970E+05	.4477E+05	-.9992E+05
0.75	.1138E+05	-.3294E+05	.1140E+05	-.3300E+05
1.00	.8931E+04	-.1181E+05	.8937E+04	-.1183E+05
1.25	.1802E+05	-.3080E+04	.1804E+05	-.3038E+04
1.50	.2679E+05	-.1115E+04	.2687E+05	-.1116E+04

Table 4. Second order pitch moment $m_y^{(2)}/\rho g a^2 A^2$ (with respect to the free surface) on uniform cylinders.

h/a	ka	m_{yq} Re	m_{yq} Im	m_{yp} Re	m_{yp} Im	m_{yt} Re	m_{yt} Im
1.0	0.25	0.0097	−0.1906	−3.4751	17.7610	−3.4654	17.5710
	0.50	0.6410	−0.3113	−2.0256	4.5736	−1.9615	4.2623
	0.75	0.1346	−0.2991	−0.4948	1.3555	−0.3602	1.0564
	1.00	0.1696	−0.2075	−0.4648	0.3174	−0.2952	0.1100
	1.25	0.1711	−0.1125	−0.8715	−0.1044	−0.7004	−0.2169
	1.50	0.1456	−0.0493	−1.2153	−0.1432	−1.0697	−0.1925
3.0	0.25	0.0231	−0.3900	−1.4726	3.8020	−1.4496	3.4120
	0.50	0.0974	−0.2289	−0.5558	−1.0018	−0.4584	−1.2307
	0.75	0.1653	−0.0299	−1.0021	−2.3006	−0.8367	−2.3305
	1.00	0.2257	0.0202	−1.9792	−2.8090	−1.7535	−2.7889
	1.25	0.2580	0.0873	−3.1615	−2.5160	−2.9035	−2.5073
	1.50	0.2393	−0.0107	−4.1937	−1.3519	−3.9544	−1.3626
10.0	0.25	0.0214	0.1476	−0.6531	−1.7621	−0.6317	−1.6145
	0.50	0.0707	0.2423	−0.8894	−4.0820	−0.8187	−3.8397
	0.75	0.1520	0.1406	−1.5668	−6.4158	−1.4148	−6.2752
	1.00	0.2269	0.0632	−2.9981	−7.3396	−2.7711	−7.2764
	1.25	0.2610	0.0172	−5.3630	−6.2119	−5.1020	−6.1948
	1.50	0.2409	−0.0094	−8.0749	−3.1548	−7.8341	−3.1642

Tables 5 and 6 are the second order surge and heave forces on a truncated cylinder with radius a and draft T/a=4 in a water depth of d/a=10. A mesh of 25 elements on the body trace Γ_B is used in this calculation. Comparison is made with Huang and Eatock Taylor's (1996) recent results at a few available frequencies. It can be seen that the present results also have a good agreement with Huang and Eatock Taylor's results.

Table 5. Comparison on second order surge forces $f_x^{(2)}/\rho gaA^2$ on a truncated cylinder of radius a and draft T/a=4 in a water depth of d/a=10, first row is the part from the first order potential f_{xq}, the second row is the part from the second order potential f_{xp} and the last row is the total force f_x.

ka	Present Results		Huang and Eatock Taylor's			
			Semi-analytical		BEM results	
	Re	Im	Re	Im	Re	Im
0.8	-0.4306	-1.4561	-0.4425	-1.4746	-0.4452	-1.4746
	1.0265	1.9767	1.0144	1.9740	1.0261	1.9702
	0.5960	0.5206	0.5719	0.4994	0.5808	0.4991
1.0	-0.8828	-1.1533				
	1.9253	1.9518				
	1.0425	0.7985				
1.2	-1.3653	-0.7721	-1.4356	-0.7970	-1.4334	-0.8024
	3.0557	1.6631	3.0406	1.6594	3.0451	1.6570
	1.6904	0.8910	1.6050	0.8629	1.6116	0.8552
1.4	-1.7242	-0.3821				
	4.0810	1.0968				
	2.3568	0.7146				
1.6	-1.8386	-0.0048				
	4.6876	0.2180				
	2.8490	0.2132				
1.8	-1.6679	0.3694				
	4.6072	-1.0689				
	2.9393	-0.6995				
2.0	-1.2595	0.7371	-1.3530	0.7652	-1.3629	0.7606
	3.9259	-2.4594	3.9052	-2.4883	3.8702	-2.4750
	2.6663	-1.7224	2.5529	-1.7233	2.5071	-1.7144

Table 7 is the second order pitch moment on the same truncated cylinder. The water depth and the mesh used are the same as for Tables 5 and 6, but calculation is run at different wave numbers for comparing with Table 4. It can be seen from the comparison between Tables 4 and 7 that the contributions from first order potential are almost the same for the uniform and truncated cylinders, especially at high frequency; but the contributions from the second order potential have a lot of difference. The reason is that the second order diffraction potential decays slowly with z-coordinate. It can also be seen that as for uniform cylinders the contribution from second order potential is the dominant part for this truncated cylinder.

Table 6. Comparison on second order total heave forces $f_z^{(2)}/\rho gaA^2$ on a truncated cylinder of radius a and draft T/a=4 in a water depth of d/a=10.

ka	Present Results		Huang and Eatock Taylor's			
			Semi-analytical		BEM results	
	Re	Im	Re	Im	Re	Im
0.8	0.0028	0.4075	0.0020	0.4047	0.0026	0.4084
1.0	0.0038	0.4113				
1.2	0.0691	0.3344	0.0690	0.3319	0.0695	0.3347
1.4	0.1908	0.2007				
1.6	0.3366	0.0445				
1.8	0.4538	-0.1037				
2.0	0.4952	-0.2301	0.4941	-0.2319	0.4960	-0.2331

Table 7. Second order pitch moment $m_y^{(2)}/\rho gaA^2$ (with respect to the free surface) on a truncated cylinder of radius a and draft T/a=4 in a water depth of d/a=10.

ka	m_{yq} Re	m_{yq} Im	m_{yp} Re	m_{yp} Im	m_{yt} Re	m_{yt} Im
0.25	0.0146	0.3363	-0.3198	-0.4347	-0.3052	-0.0984
0.50	0.0647	0.2712	-0.4676	-1.6493	-0.4028	-1.3781
0.75	0.1500	0.1462	-1.0222	-2.5751	-0.8722	-2.4289
1.00	0.2268	0.0634	-2.0075	-3.0066	-1.7808	-2.9432
1.25	0.2613	0.0168	-3.2300	-2.6530	-2.9688	-2.6362
1.50	0.2410	-0.0097	-4.3187	-1.4233	-4.0777	-1.4330

6.2 S_{1mn} and S_{2mn} functions

To accelerate the convergence of the integration on the free surface, this report suggested a forward prediction method for compute the functions S_1 and S_2 after having got the functions at a position. Before applying the method for practical calculation, some examinations on the forward prediction method have to be carried out. Here an examination is made on a uniform cylinder of radius a in a water depth of d/a=10. Wave number ka is 0.5. The examination is only made on the zero Fourier mode and *0*th, *1*st, *10*th and *50*th eigen-modes of the functions. The step length used in the forward prediction is 0.01257a.

Figure 3 shows the comparison of function S_1 by the direct integration and forward prediction method. For the zero eigen-mode, the forward prediction method is to compute the function at r=a by the direct integration method, then to apply the forward prediction method successively. From Figs. 3-A and 3-B we can see that even though we have applied the forward prediction method for 2000 steps, the results are still the same with the one from the direct integration method. We can not see any difference between the results from the two different methods.

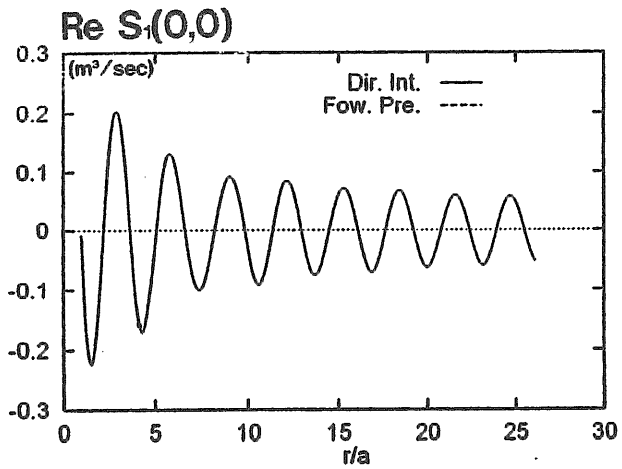

Fig. 3-A Real part of $S_1(0,0)$

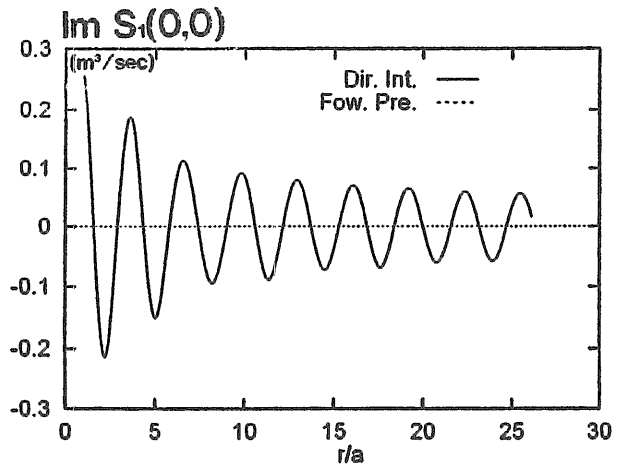

Fig. 3-B Imaginary part of $S_1(0,0)$

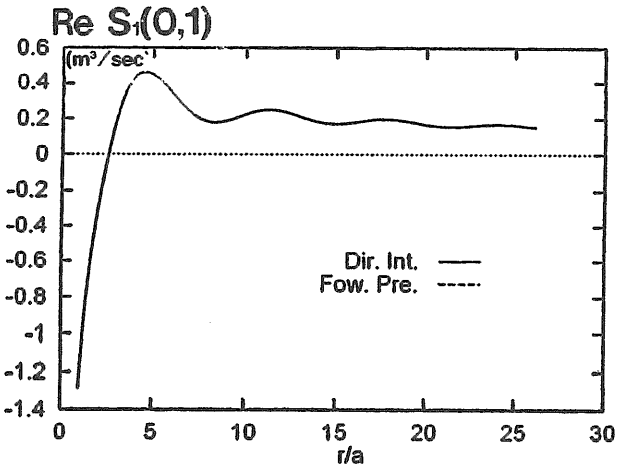

Fig. 3-C Real part of $S_1(0,1)$

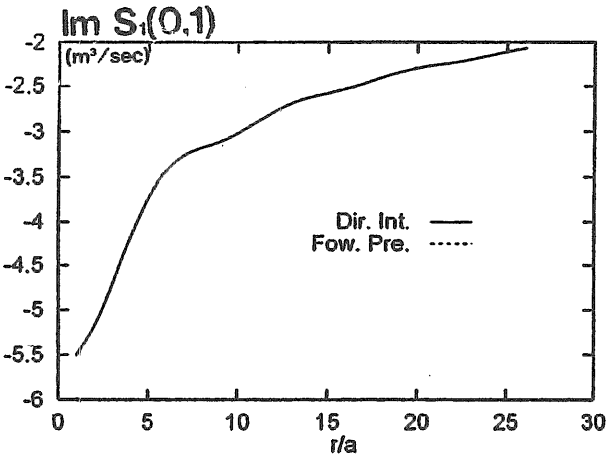

Fig. 3-D Imaginary part of $S_1(0,1)$

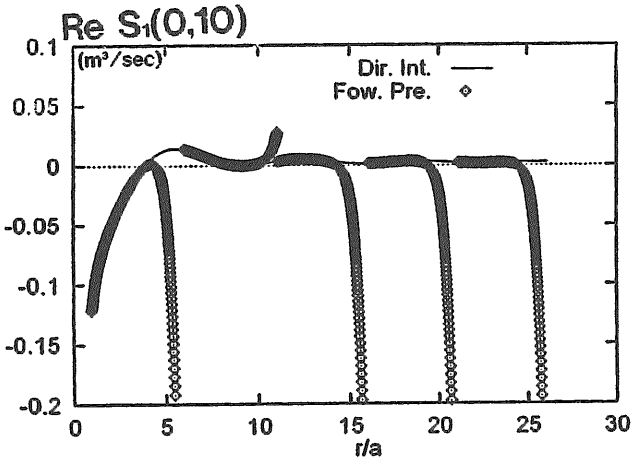

Fig. 3-E Real part of $S_1(0,10)$

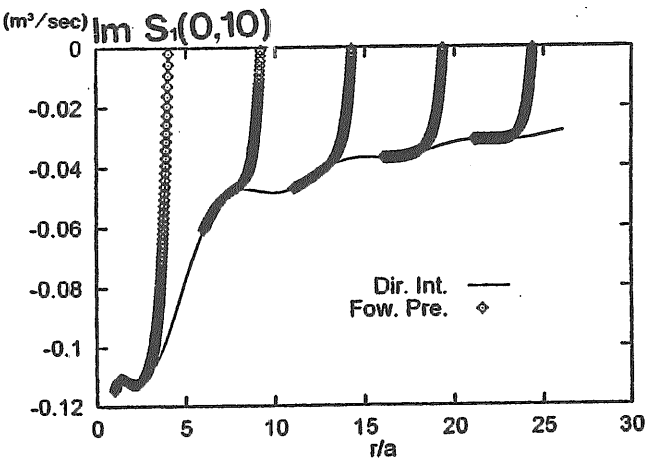

Fig. 3-F Imaginary part of $S_1(0,10)$

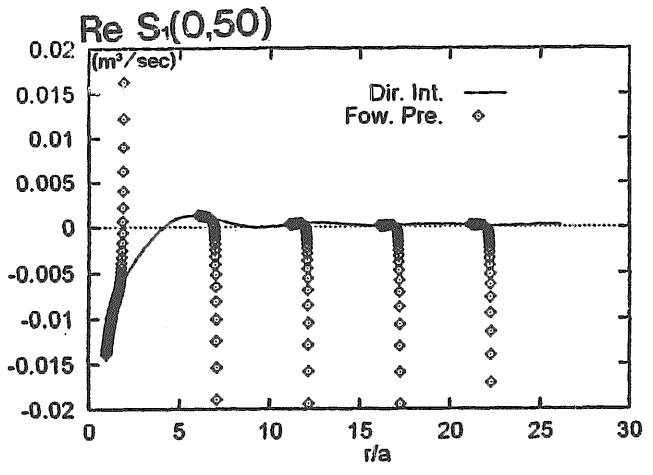

Fig. 3-G Real part of $S_1(0,50)$

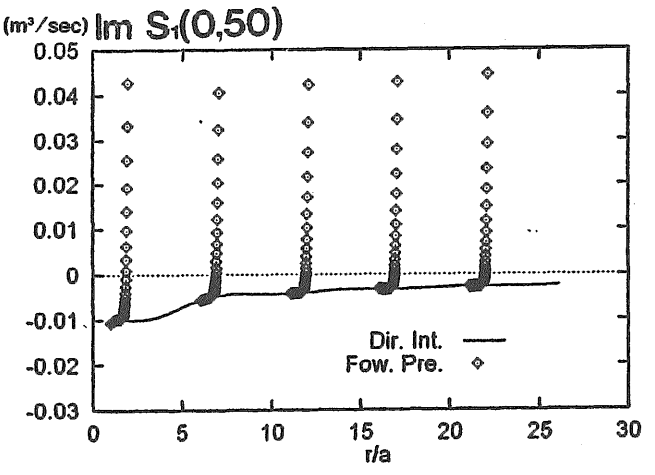

Fig. 3-H Imaginary part of $S_1(0,50)$

Figure 3. Examination on the methods, the direct integration method and forward predict method, for computing $S_1(m,n)$ for a uniform cylinder of radius a in a water depth of d/a=10; wave number ka=0.5.

For the *1*st, *10*th and *50*th eigen-modes of S_1 we apply the forward prediction method for every 400 steps, then correct it by the direct integration method. From the Figs. 3-C – 3-H, we can seen that for the first eigen-mode the forward prediction method can give accurate results in the 400 steps. For the *10*th eigen-mode the forward prediction method can give accurate results for some steps. After that the method will lose accuracy and diverges quickly. For the *50*th mode, the available distance to predict is shorter than the *10*th mode and the prediction method diverges more easily. The reason for long predictable length for low eigen-modes is that actually the dominating factor is the variable $\kappa_n \Delta r$ in modified Bessel functions rather than the distance Δr itself. Furthermore, the predictable length is also affected by a truncation-error tolerance

$$\int_{r_1}^{r_1+\Delta r} K_m(\kappa_n r) q_D^{(2)} r\,dr \Big/ \left[\int_{r_0}^{r_1} K_m(\kappa_n r) q_D^{(2)} r\,dr + \int_{r_1}^{r_1+\Delta r} K_m(\kappa_n r) q_D^{(2)} r\,dr\right] < Er \qquad (51)$$

used in calculation of the function S_1 by the direct integration method. In the present calculation, a tolerance of 1.0E-04 is applied.

Figure 4 shows the comparison between the direct integration and forward prediction method for the function S_2. The steps for the forward prediction method are exactly the same as for the function S_1. It can be seen that for the all of the four eigen-modes, the results from the two methods are exactly the same. The reason is that the forward prediction method for the function S_2 is successively accumulating, rather than subtracting as for S_1.

In practical calculation, the method used in computing S_1 is that firstly the direct integral method is used to compute the accurate values, then the forward prediction method is used to predict them for a certain steps. Then, the direct integration method is used again to remove the error accumulated in the forward prediction method and to guarantee that the forward prediction method can be used for the next loop. The numbers of steps used in the forward prediction method are different for each models, and are determined by a previous

numerical examination. This calculation loop is used repeatedly until the second order potential is obtained in the whole desired area.

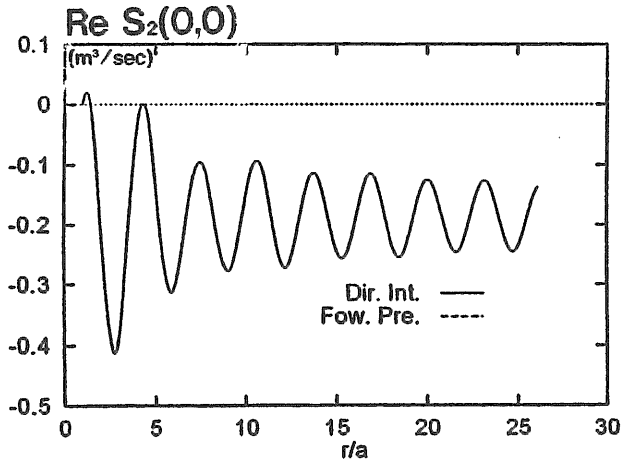

Fig. 4-A Real part of $S_2(0,0)$

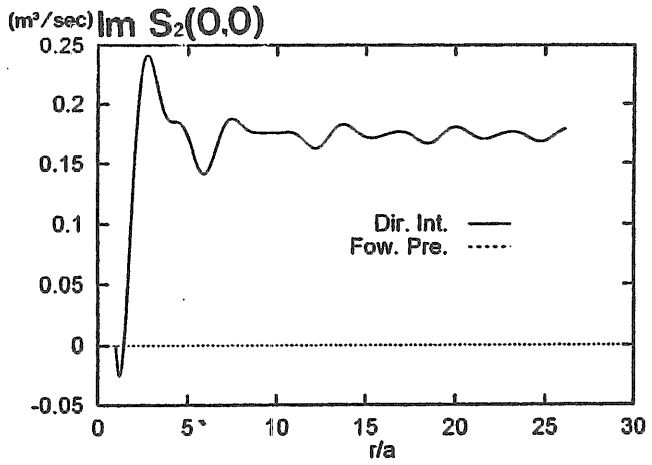

Fig. 4-B Imaginary part of $S_2(0,0)$

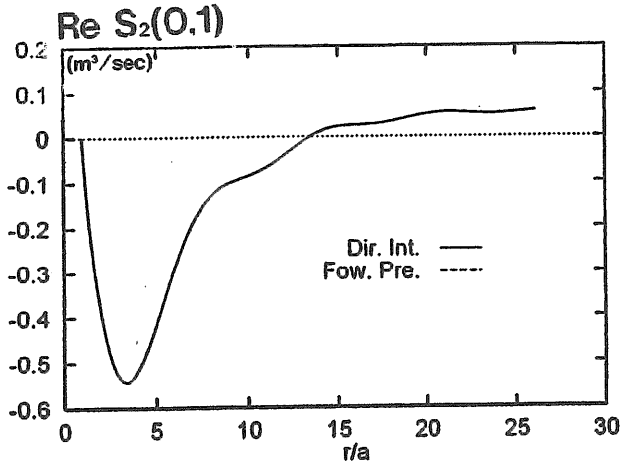

Fig. 4-C Real part of $S_2(0,1)$

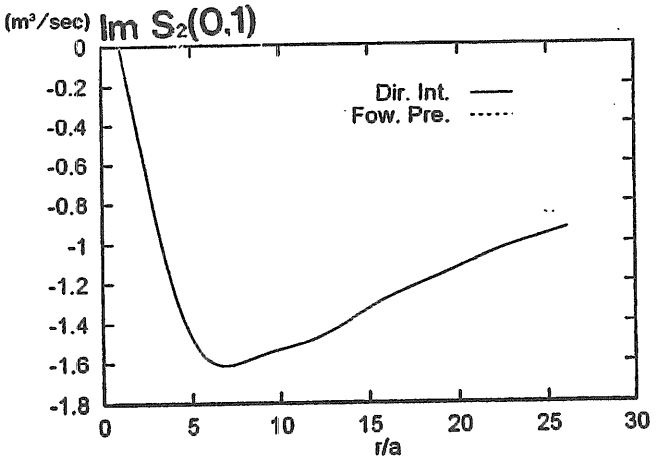

Fig. 4-D Imaginary part of $S_2(0,1)$

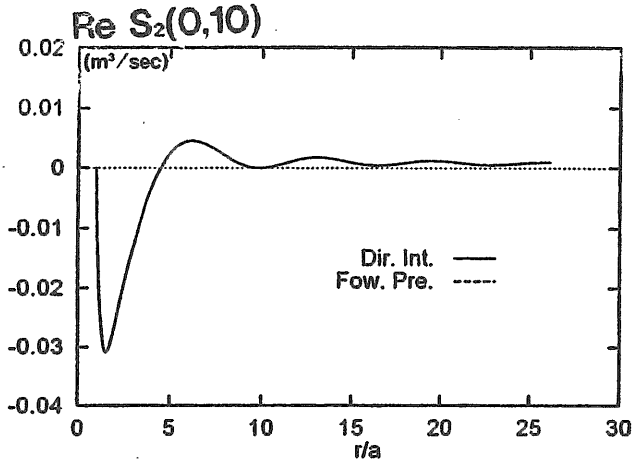

Fig. 4-E Real part of $S_2(0,10)$

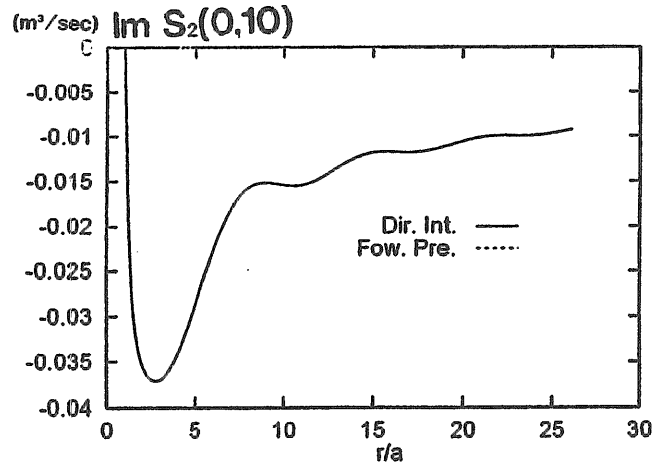

Fig. 4-F Imaginary part of $S_2(0,10)$

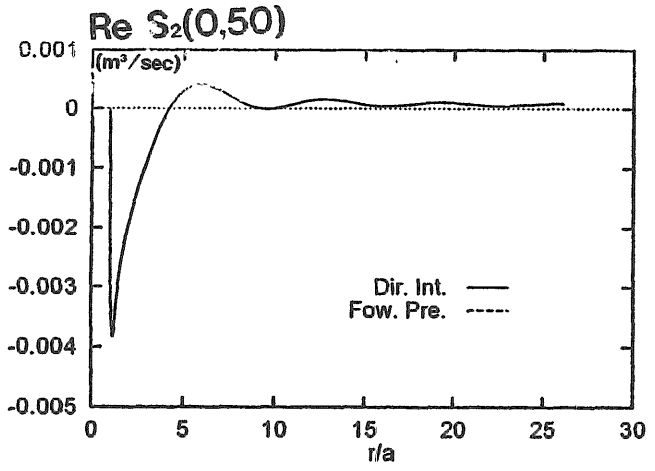

Fig. 4-G Real part of $S_2(0,50)$

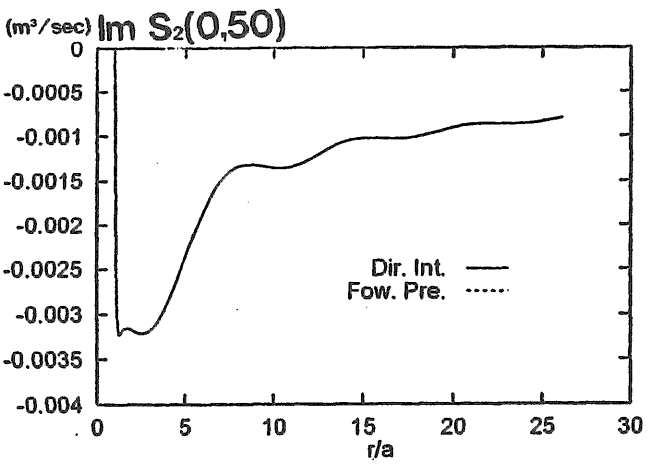

Fig. 4-H Imaginary part of $S_2(0,50)$

Figure 4. Examination on the methods, the direct integration method and forward predict method, for computing $S_2(m,n)$ for a uniform cylinder of radius a in a water depth of d/a=10; wave number ka=0.5.

6.3 Second order potential on the free surface

After having gotten those two functions S_1 and S_2, we can obtain the second order potential in fluid domain easily. Figure 5 shows the comparison of present results of second order diffraction potential on the free surface with Malenica's (1994) results. The comparison is made on the *0*th, *1*st and *5*th Fourier modes of diffraction potential, and also the radial derivative of the potential, which is obtained by a simple backward numerical differentiation.

It can be seen from the figures that the curves of potentials are very smooth, but the ones of radial derivatives have some noises. This is due to that some errors have been accumulated in the forward prediction method when the direct integration method is used to get an accurate value for the next computing loop. For the potential itself, this error is very small and can be tolerated. But, since the step is very small, the error of derivative will be quite big in the local area. To obtain a smooth result for the radial derivative, we have to use less steps to predict, or use other differentiation scheme.

From the comparison with Malenica's semi-analytic solution, it can be seen that for all the three modes of both potential and its derivative, the present results have a good agreement with Malenica's.

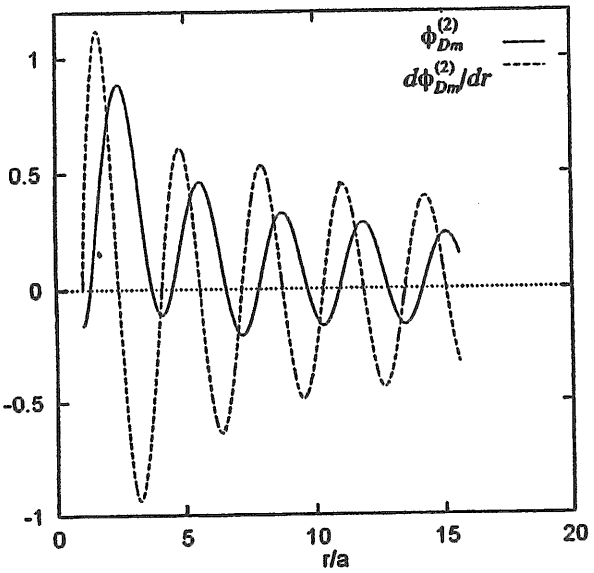

Fig. 5-A Real part of present results of $\phi_{Dm}^{(2)}$ and $d\phi_{Dm}^{(2)}/dr$, $m=0$

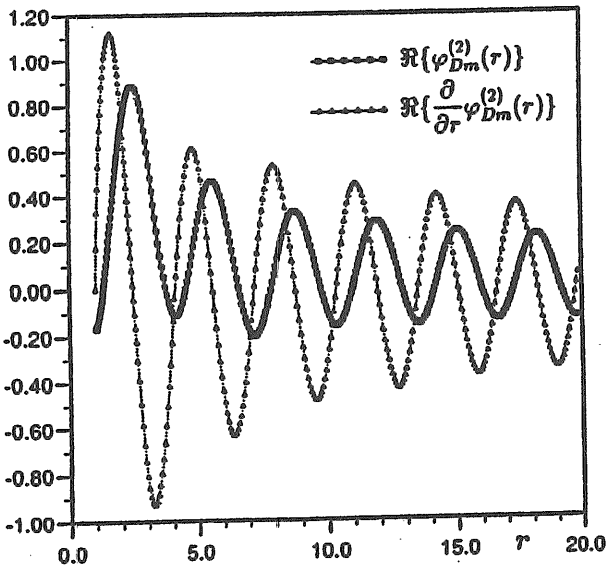

Fig. 5-B Real part of Malenica & Molin's results of $\phi_{Dm}^{(2)}$ and $d\phi_{Dm}^{(2)}/dr$, $m=0$

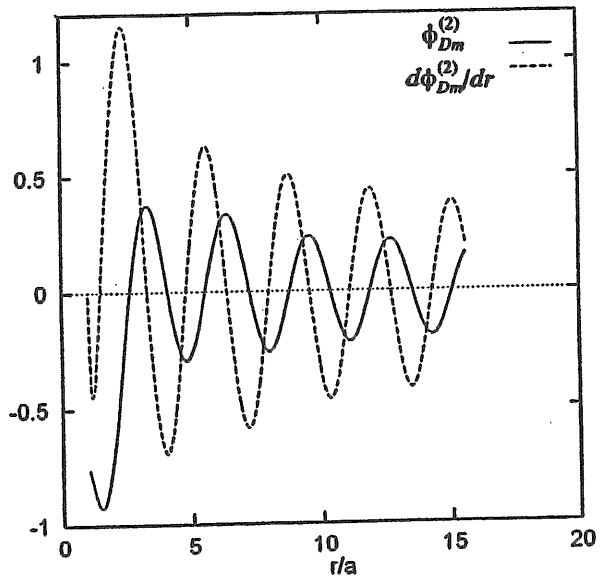

Fig. 5-C Imaginary part of present results of $\phi_{Dm}^{(2)}$ and $d\phi_{Dm}^{(2)}/dr$, $m=0$

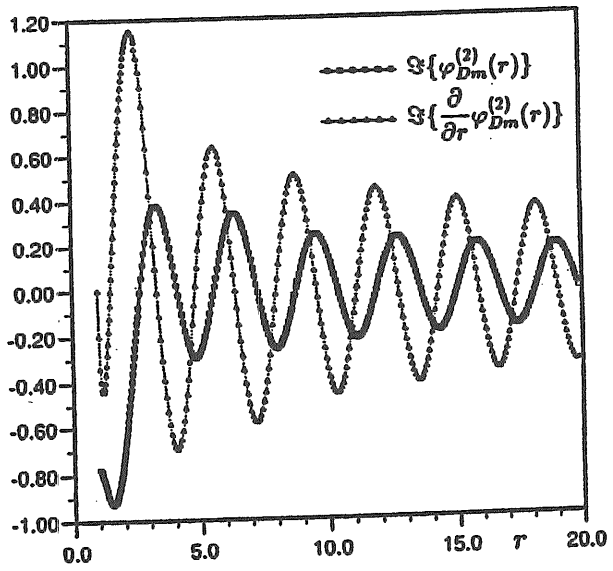

Fig. 5-D Imaginary part of Malenica & Molin's results of $\phi_{Dm}^{(2)}$ and $d\phi_{Dm}^{(2)}/dr$, $m=0$

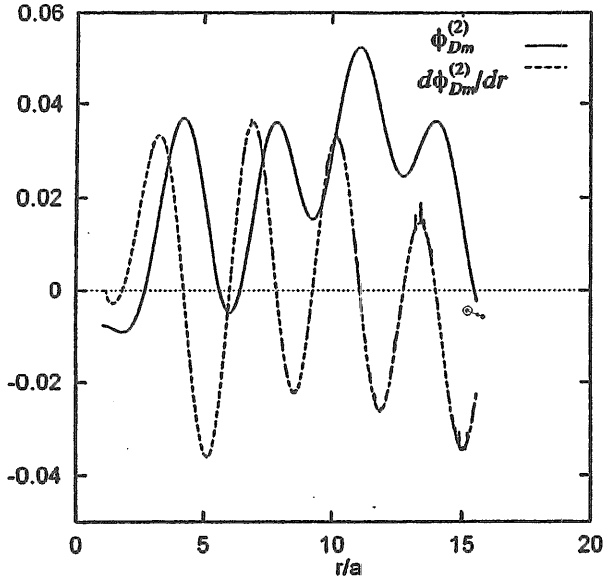

Fig. 5-E Real part of present results of $\phi_{Dm}^{(2)}$ and $d\phi_{Dm}^{(2)}/dr$, $m=1$

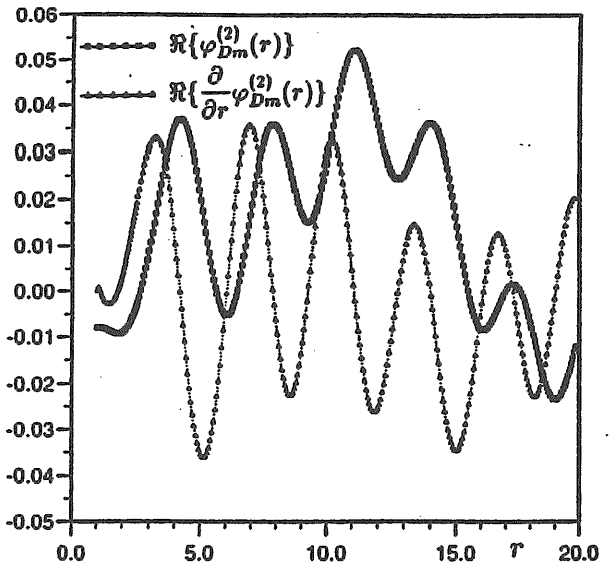

Fig. 5-F Real part of Malenica & Molin's results of $\phi_{Dm}^{(2)}$ and $d\phi_{Dm}^{(2)}/dr$, $m=1$

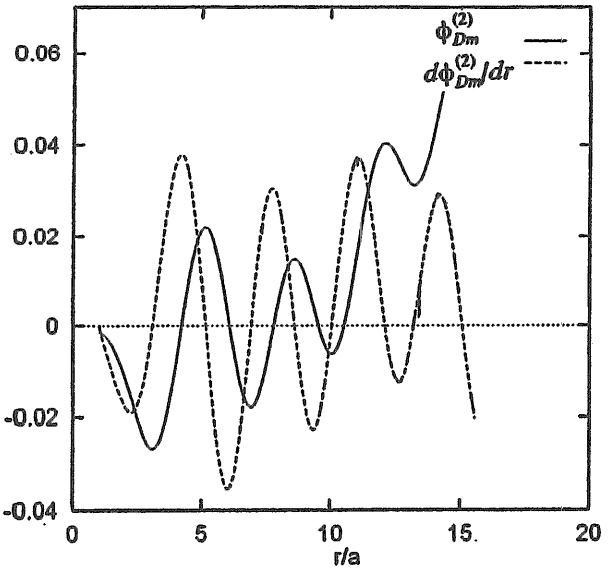

Fig. 5-G Imaginary part of present results of $\phi_{Dm}^{(2)}$ and $d\phi_{Dm}^{(2)}/dr$, $m=1$

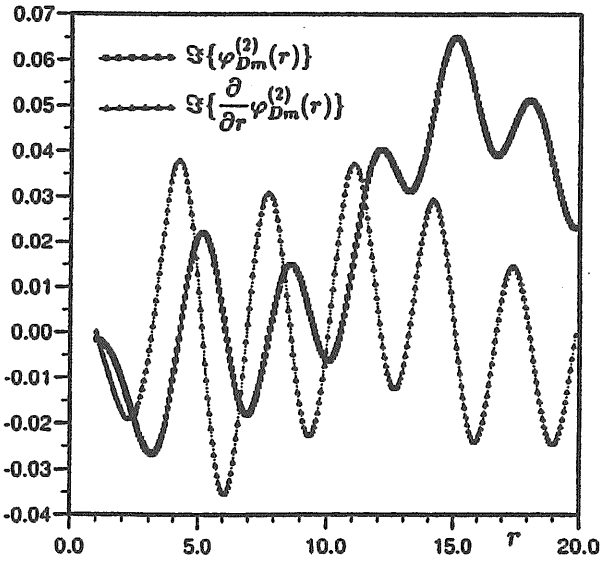

Fig. 5-H Imaginary part of Malenica & Molin's results of $\phi_{Dm}^{(2)}$ and $d\phi_{Dm}^{(2)}/dr$, $m=1$

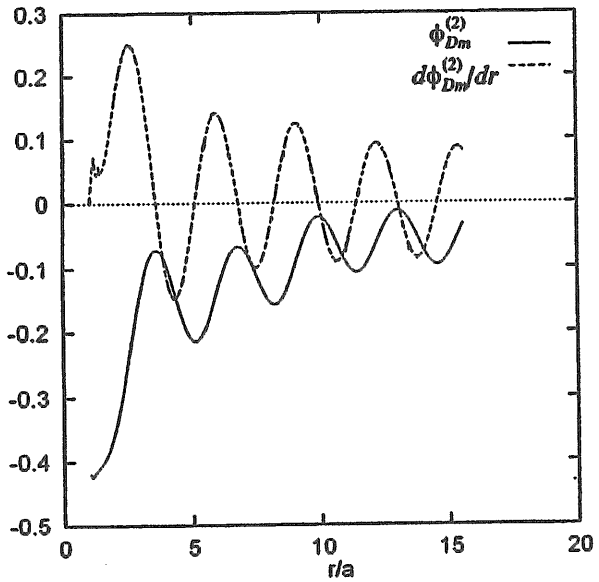

Fig. 5-I Real part of present results of $\phi_{Dm}^{(2)}$ and $d\phi_{Dm}^{(2)}/dr$, $m=5$

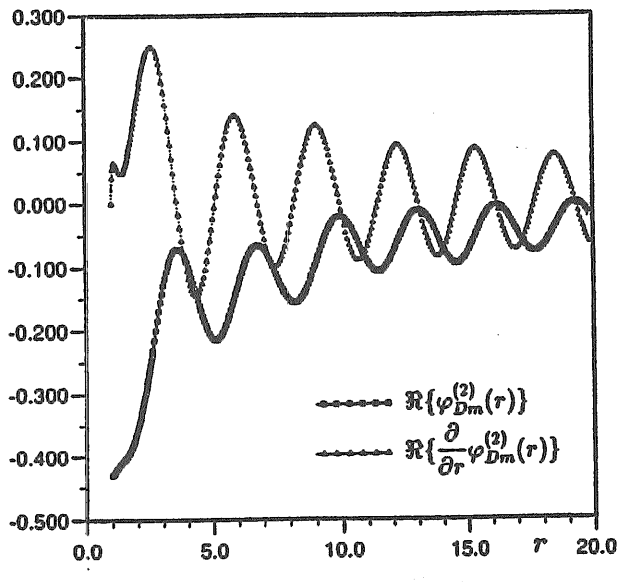

Fig. 5-J Real part of Malenica & Molin's results of $\phi_{Dm}^{(2)}$ and $d\phi_{Dm}^{(2)}/dr$, $m=5$

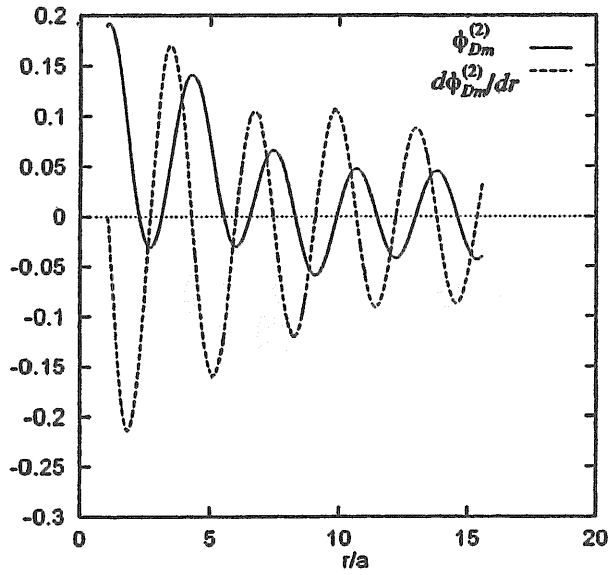

Fig. 5-K Imaginary part of present results of $\phi_{Dm}^{(2)}$ and $d\phi_{Dm}^{(2)}/dr$, $m=5$

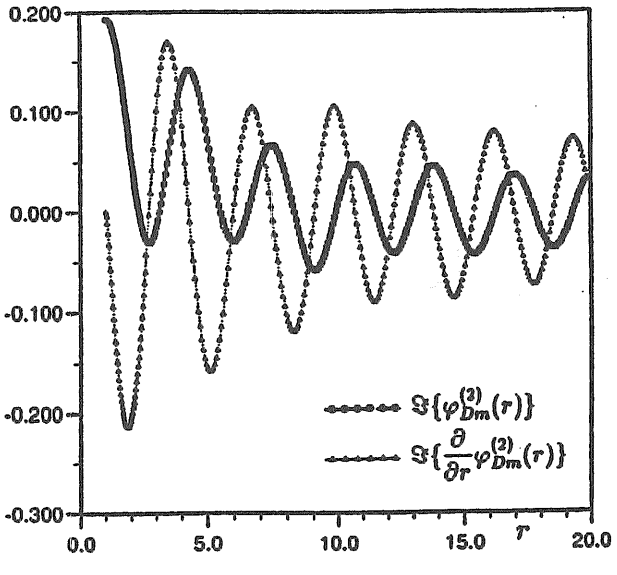

Fig. 5-L Imaginary part of Malenica & Molin's results of $\phi_{Dm}^{(2)}$ and $d\phi_{Dm}^{(2)}/dr$, $m=5$

Figure 5. Examination on second order diffraction potential and its radial derivative on the free surface for a uniform cylinder of radius a in a water depth of d/a=10; wave number ka=0.5.

6.4 Wave elevation

Figure 6 shows the second order wave elevation from the second order diffraction potential around a uniform cylinder. The water depth d/a=10; waves direct to positive x- direction with a wave number of ka=0.5. The pictures are plotted at every time step of one *16*th of wave period T_p ; that is one 8th of the second harmonic oscillation. Figure 7 shows the second order wave elevation from the diffraction potential around a truncated cylinder. The draft of the cylinder is T/a=1.0, and the water depth and the wave conditions are the same as for the uniform cylinder. From the comparison of figures 6 and 7, it can be seen that the diffraction wave from the uniform cylinder is much higher than the one from the truncated cylinder. It means that at present wave frequency the diffraction from the lower part of the cylinder is still quite strong, and uniform cylinders will not make a good substitution for truncated cylinders when considering ringing phenomenon in long waves.

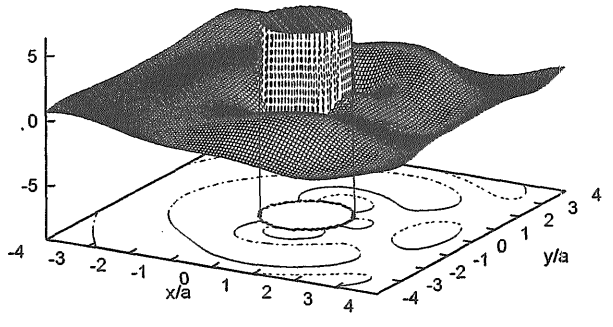

Fig. 6-A Wave elevation at t=0.0T_p

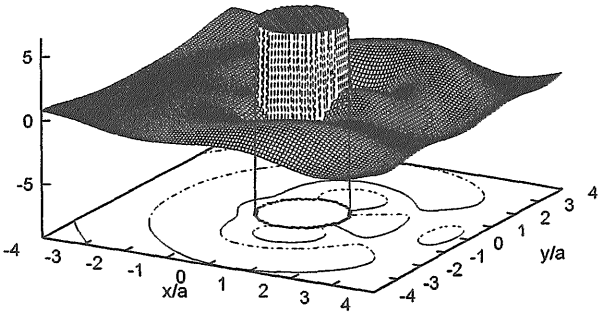

Fig. 6-B Wave elevation at t=T_p/16

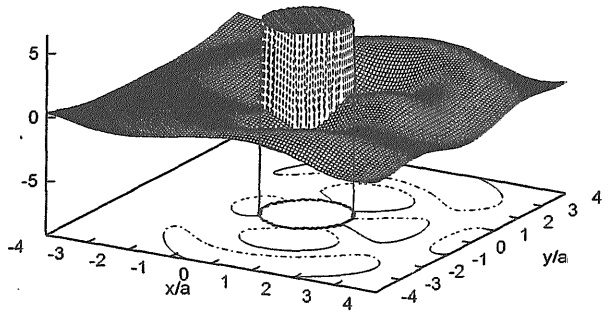

Fig. 6-C Wave elevation at t=2T_p/16

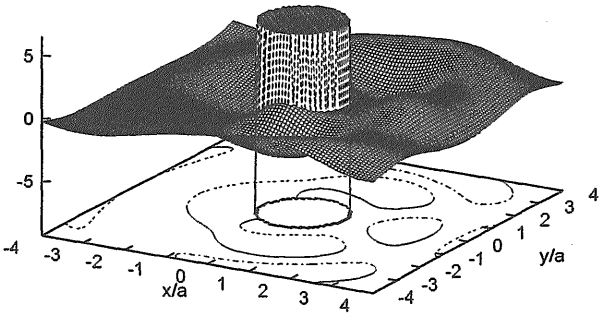

Fig. 6-D Wave elevation at t=3T_p/16

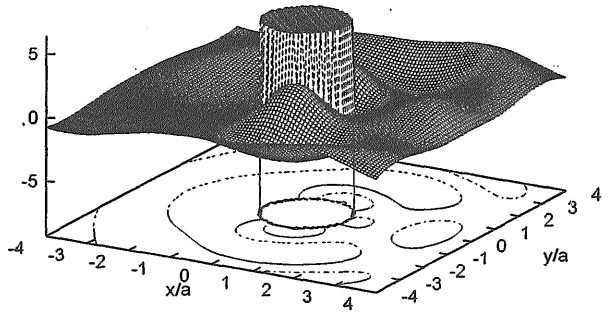

Fig. 6-E Wave elevation at t=4T_p/16

Figure 6. Wave elevation from second order diffraction potential around a uniform cylinder of radius a in a water depth of d/a=10; wave number ka=0.5.

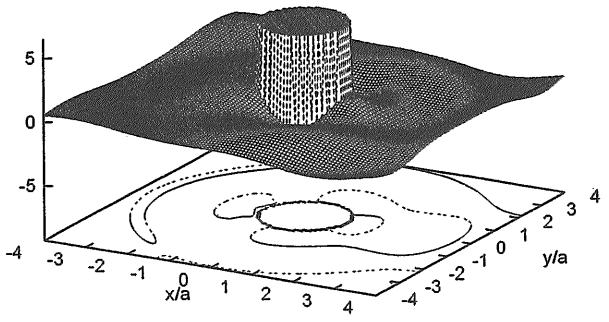

Fig. 7-A Wave elevation at t=0.0T_p

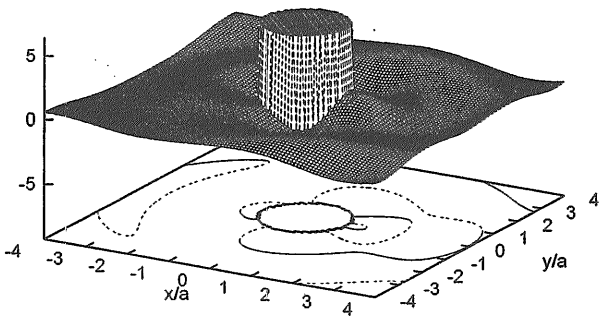

Fig. 7-B Wave elevation at t=T_p/16

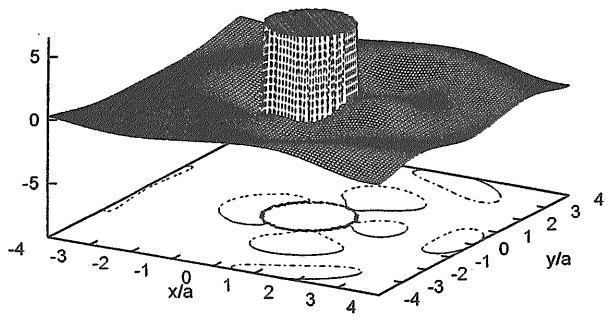

Fig. 7-C Wave elevation at t=2T_p/16

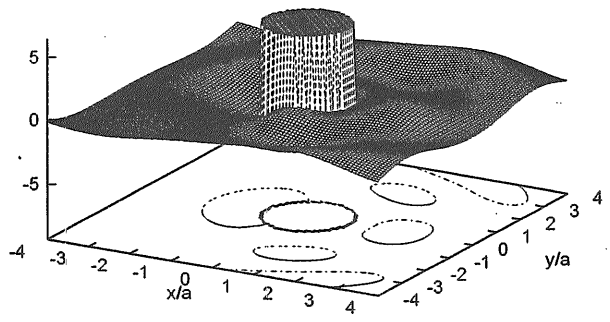

Fig. 7-D Wave elevation at t=3T_p/16

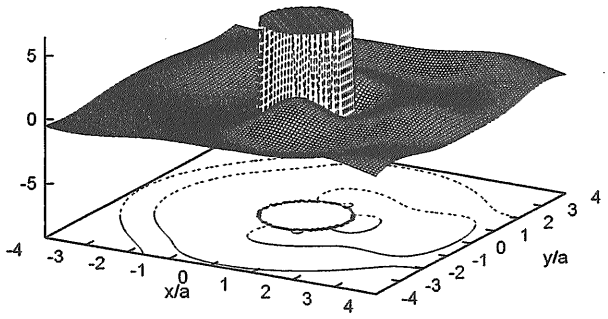

Fig. 7-E Wave elevation at t=4T_p/16

Figure 7. Wave elevation from second order diffraction potential around a truncated cylinder with radius a and draft T/a=1.0 in a water depth of d/a=10 ; wave number ka=0.5.

7. Conclusions

A complete second order diffraction solution has been derived for a vertical revolution body. The method is based on using the ring-source integral equation. The emphasis was laid on the quick calculation of the integration on the free surface. It can also be easily expanded for 3D arbitrary bodies. The following conclusions can be summarized.

1. The report derives an new integral equation for revolution bodies with vertical axes. The integral equation can cancel the leading term of the singularity in derivative of the ring- source. Remaining low order

singularities are dealt with by a coordinate transform.

2. For the integration on the free surface, a forward prediction method is proposed for computing the second order potential in a big area. By this method the integration on the free surface for different source points is carried out outward from the body by successively subtracting and accumulating the quadratures in each forward moving step, rather than integrating on the whole free surface for each point individually. This is very significant for the calculation of third order forces, for which the second order potential is needed on the whole free surface or in a very big area.

3. Attention is also paid for dealing with the integration of singularities on the free surface. In this report, a method is proposed to add and subtract an integration of the singular kernel of the ring-source in the nearby of the source point. Thus, the infinite summation of the ring-source can be truncated at a big number, and integrations with the singular kernel can be localized to lower computing burden.

4. Numerical examination is made on the forward prediction method for functions S_1 and S_2 by comparing with the direct integration method. The numerical results show that for S_2 the forward prediction method is uniformly available; for S_1, the forward prediction method is uniformly available for its zero eigen-mode, but for other eigen-modes it can only be used in certain steps. Numerical results also show that for lower eigen-modes, the predictable distance is longer; and for higher eigen-modes, the distance is shorter.

5. A predicting and correcting method is used for computing S_1 and S_2 repeatedly, which is to predict them by the forward prediction method for a certain steps, then correct them by the direct integration method. The number of predicting steps is determined by previous numerical examination, and is different for each modes. The method can save a lot of computing effort, and can be used to compute the second order potential over the big area, including the free surface.

6. Comparison with other published results is made on second order force on different cylinders and the second order diffraction potential to validate the numerical code. Comparison shows that the present results have a good agreement with others. The program is also used to compute pitch moment on the uniform and truncated cylinders. Results show that the difference is evident between the moments on uniform and truncated cylinders in the same water depth.

7. The numerical code has been used to compute the wave elevation from second order diffraction potential around uniform and truncated cylinders in the same water depth and the same wave conditions. The results shows that at the calculation frequency, the second order wave diffractions from the two cylinders are quite different. It suggests that we should be careful to use an array of uniform cylinders as a substitution of actual TLPs when considering ringing phenomenon in long waves.

8. After getting the second order potential on the free surface by the present method for axisymmetric bodies, we can obtain the third order forcing term on the free surface. Then, the calculation of third order force is straightforward, such as by an indirect method for second order forces.

This work is partly supported by Japan Science and Technology Promotion Foundation, Japan Science and Technology Agency Fellowship, and the National Natural Science Foundation of China.

References

1. Chau F.P. and Eatock Taylor, R., Second-order wave diffraction by a vertical cylinder, Jour. Fluid Mech., Vol.240, pp.571-599 (1992).
2. Eatock Taylor, R. and Chau F.P., Wave diffraction–some developments in linear and non-linear theory, Jour. Offshore Mech. and Arctic Engng, Vol.114, pp.185-94 (1992).
3. Eatock Taylor, R. and Hung, S.M., Second order diffraction forces on a vertical cylinder in regular waves, Applied Ocean Res. Vol.9, pp.19-30 (1987).
4. Fenton, J.D., Wave forces on vertical bodies of revolution, Jour. Fluid Mech., Vol.85, pp.241-255 (1978).
5. Huang, J.B. and Eatock Taylor, R., Semi-analytical solution for second-order wave diffraction by a truncated circular cylinder in monochromatic waves, Vol.319, pp.171-196 (1996).
6. Hulme, A., A ring source integral equation method for the calculation of hydrodynamic forces exerted on floating bodies of revolution, J. Fluid Mech. Vol.128,pp.387-412 (1983).
7. Hunt, J.N. and Baddour, R.E. The diffraction of nonlinear progressive waves by a vertical cylinder, Quart. J. Mechanics and Applied mathematics, Vol.34, No.1, pp.69-88 (1981)
8. Kim, M.H. and Yue, D.K.P., The complete second-order diffraction solution for an axisymmetric body. Part 1. Monochromatic incident waves, Jour. Fluid Mech., Vol.200, pp.235-264 (1989).
9. Kriebel D.L., Nonlinear Wave Interaction with a Vertical Circular Cylinder. Part 1:Diffraction Theory, Ocean Engineering, Vol.17, No.4, pp345-377 (1990).
10. Malenica, S., Diffraction de troisieme order et interaction houle-courant pour un cylindre vertical en profonfeur finie. PhD dissertation, Paris 6 University (in French) (1994).
11. Malenica, S. and Molin, B., Third-harmonic wave diffraction by a vertical cylinder, Jour. Fluid Mech., Vol.302, pp.203-229 (1995).
12. Molin, B., Second-order diffraction loads upon three dimensional bodies, Applied Ocean Res., Vol.1, pp.197-202 (1979).
13. Newman, J.N., The second-order wave force on a vertical cylinder, to be published in Jour. Fluid Mech., (1996).
14. Telles, J.C.F., A self-adaptive co-ordinate transformation for efficient numerical evaluation of general boundary element integrals, Intl. J. Numer. Meth. Engng., Vol.24, 959-973 (1987).
15. Teng, B. and Eatock Taylor, R., New higher-order boundary element methods for wave diffraction/radiation, Applied Ocean Research, Vol.17, pp.71-77 (1995).
16. Teng, B and Kato, S., An effective method for second order potential–towards the calculation of third order forces, 11th Workshop on Water Waves and Floating Bodies, Hamburg (1996).
17. Watson, G.N., Theory of Bessel Functions, Cambridge University Press (1966).
18. Kato,S. and et al., Ringing Response of a Tension Leg Platform -Theoretical and experimental analyses of a third order force on TLP -, Journal of Naval Anchitecture of Japan, Vol.180, pp.175-192 (1996)